Article

The Effects of Rainfall, Soil Type and Slope on the Processes and Mechanisms of Rainfall-Induced Shallow Landslides

Yan Liu [ID], Zhiyuan Deng and Xiekang Wang *[ID]

State Key Laboratory of Hydraulics and Mountain River Engineering, Sichuan University, Chengdu 610065, China; liuyan2021scu@gmail.com (Y.L.); dengzhiyuan2019@163.com (Z.D.)
* Correspondence: wangxiekang@scu.edu.cn

Abstract: Landslides are a serious geohazard worldwide, causing many casualties and considerable economic losses every year. Rainfall-induced shallow landslides commonly occur in mountainous regions. Many factors affect an area's susceptibility, such as rainfall, the soil, and the slope. In this paper, the effects of rainfall intensity, rainfall pattern, slope gradient, and soil type on landslide susceptibility are studied. Variables including soil volumetric water content, matrix suction, pore water pressure, and the total stress throughout the rainfall were measured. The results show that, under the experimental conditions of this paper, no landslides occurred on a 5° slope. On a 15° slope, when the rainfall intensity was equal to or less than 80 mm/h with a 1 h duration, landslides also did not happen. With a rainfall intensity of 120 mm/h, the rainfall pattern in which the intensity gradually diminishes could not induce landslides. Compared with fine soils, coarser soils with gravels were found to be prone to landslides. As the volumetric water content rose, the matrix suction declined from the time that the level of infiltration reached the position of the matrix. The pore water pressure and the total stress both changed drastically either immediately before or after the landslide. In addition, the sediment yield depended on the above factors. Steeper slopes, stronger rainfall, and coarser soils were all found to increase the amount of sediment yield.

Keywords: landslides; artificial rainfall; grain size; rainfall pattern; pore water pressure

1. Introduction

Landslides refer to the geological phenomenon of rock and soil mass sliding along a slope, these are a type of natural hazard that is widely distributed throughout the world [1,2]. Landslides cause tens of billions of dollars of economic losses and serious casualties worldwide every year [3]. In areas with complex geological conditions, landslides occur more frequently [4–7].

In mountain regions, landslides are often triggered by intensive rainfall [8,9]. Rainfall and infiltration enhance moisture content, which further decreases the matrix suction and soil shear strength [10,11]. Rainfall characteristics are often used as criteria for landslide occurrence [12,13]. The rainfall's intensity and pattern influence the characteristics of landslides [14–16]. To date, there have been many studies on the effects of rainfall on landslides. Research methods include in situ experiments, laboratory experiments, and numerical simulations [17,18]. The artificial rainfall test is an effective method when used to study rainfall-induced landslides [19].

Slopes with different soil compositions respond differently to rainfall. Fine particle migration leads to pore blockage [20] and the soil composition of slopes is closely related to their landslide susceptibility. Research has showed that a prerequisite for landslides to occur is that the clay percentage of the soil is higher than 2.5% [21]. The soils in a region where earthquakes happen often have many coarse particles, such as gravel. The proportion of gravel in soils has a great influence on the density and void ratio, which determines the timing and type of landslides [22]. The failure mode is closely related to the grain size [23].

The type of landslide is usually a gully failure when small gravel content is present and usually a "layer-by-layer sliding" failure when large gravel content is present [24].

Rainfall and infiltration change the soil characteristics greatly [25]. Some physical qualities of the soil change during rainfall, such as the water content, matrix suction, pore water press, and total stress [26,27]. The volumetric water content is the ratio of the volume of water to the unit volume of soil and it increases during rainfall. Matrix suction is a sensitive parameter when unsaturated soils encounter rainfall and it is differently affected for soils with varying levels of rainfall infiltration [28,29]. The pore water press increases during rainfall and reduces the soil's shear strength. Slopes with greater inclination have larger pore water press [30]. Total stress is the basis of stability analyses that are used for calculating the factor of safety [31]. However, all of the above studies measured one or several of the physical quantities of the soil and lacked a comprehensive reflection of the changes in soil properties during landslides.

The landslide is a typical example of gravity-based erosion. The sediment yield of landslides varies with the presence of a number of factors [32,33]. The time scale of the impact of a landslide on the sediment yield in the basin is large. To comprehensively analyze sediment transport, it is necessary to investigate the landslide history of the basin for at least the preceding 100 years [34]. The landslide sediment yield of soil that is affected by an earthquake under rainfall has been studied and quantified [35]. One model that is used to express the contribution of shallow landslides to sediment yield as a rainfall characteristic function has been established [36]. Another model called SHEETRAN was established in order to analyze the impact of rainfall on landslides and sediment transport. It was applied to the Valsassina Basin, which is a wide glaciated valley with a U-shaped profile. The superficial deposits that are found on the valley's slopes consist of calcareous-dolomitic chaotic material with loose and sharp-edged fragments. [37–39]. The effects of rainfall on sediment yield are obvious and the sediment yield increases with an increase in the gravel percentage [40,41].

Therefore, the purpose of this paper is to make clear how each factor influences landslide occurrences. A series of physical model tests that were carried out by an artificial rainfall system was performed in order to investigate the process and mechanics of slope failure. The rainfall intensity, rainfall pattern, soil type, and slope gradients each play a unique role in slope stability. In the process, the main physical parameters of the soil, including volumetric water content, matrix suction, pore water pressure, and total stress, were all measured. Based on the detailed measured data, we were able to derive the relationship between these physical qualities and the timing of landslides. Moreover, the sediment yield of landslides was quantified and the dependence of the yield on the test variables was analyzed. The present experimental results contribute to improving the understanding of landslide mechanisms and mitigating landslide disasters.

2. Materials and Methods

2.1. Experimental System

The artificial rainfall test site that was used in this study is located in the State Key Laboratory of Hydraulics and Mountain River Engineering of Sichuan University. The system is composed of a reservoir, water pump, water delivery pipe, rain gauge, electromagnetic flowmeter, nozzle, and valve (Figure 1). It is controlled by computer software and can be self-adjusted automatically. When the automatic adjustment mode is turned on, the water pressure and valve opening can be adjusted automatically in order to hold or change the rainfall intensity. A water content sensor, tensiometer, earth press cell, and pore water pressure sensor were used in the test (Figure 2c). The flume that was used for the test was made of impermeable transparent polymer plastic material, with a length of 2 m, a width of 0.3 m, and a height of 0.8 m. The flume was placed horizontally. The three slope angles that were set in this research were 5°, 15°, and 30°. The flume, soil, and instruments that were used are shown in Figure 2.
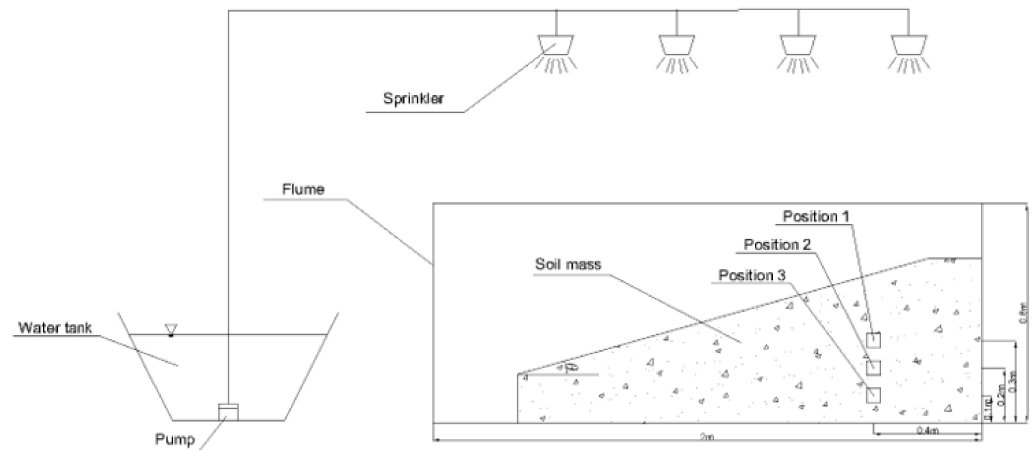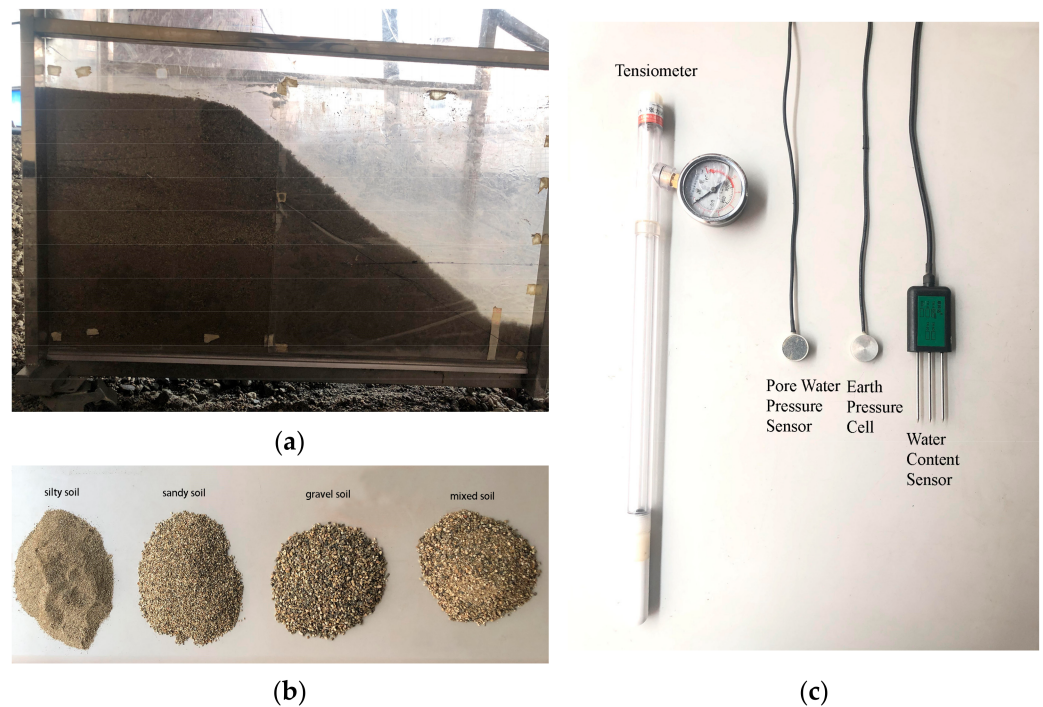
Figure 1. Sketch of experimental setup.

(a)

(b)

(c)

Figure 2. Tested samples and experimental apparatus: (**a**) side view of the slope; (**b**) soil samples; (**c**) measuring apparatuses.

2.2. Experimental Program

The experiment was set up with four variables: rainfall intensity, rainfall pattern, soil type, and slope gradient (Table 1). Each variable was changed only when the other variables were kept constant in order to study the relationship between that variable and landslide susceptibility. Four values of 40 mm/h, 80 mm/h, 120 mm/h, and 160 mm/h were taken for the rainfall intensity variable when the rainfall pattern was uniform (Tests no. 1–4). The rainfall pattern variable was set to I, II, III, and IV (test no. 5–7 and 3), these rainfall intensity change processes are shown in Figure 3.

In tests no. 8–10 and 3, four soil types were used. Three of the soil types were mainly composed of silt, sand, and gravel, respectively, and the mixed type was a 1:1:1 mixture of the aforementioned three. The soil compositions were set according to the common soil types that are seen in Min Jiang River basin in southwest China. The soil that was used for the tests was collected in nature through systemic screening and mixed. The soil

compositions are listed in Table 2 and the grain size distribution curves of the soil types are shown in Figure 4.

Table 1. Test variables.

Test No.	Rainfall Intensity (mm/h)	Rainfall Pattern	Soil Type	Slope Gradient (°)
1	40	IV	Mixed soil	15
2	80	IV	Mixed soil	15
3	120	IV	Mixed soil	15
4	160	IV	Mixed soil	15
5	120	I	Mixed soil	15
6	120	II	Mixed soil	15
7	120	III	Mixed soil	15
8	120	IV	Silty soil	15
9	120	IV	Sandy soil	15
10	120	IV	Gravel soil	15
11	120	IV	Mixed soil	5
12	120	IV	Mixed soil	30

(**a**)   (**b**)   (**c**)   (**d**)
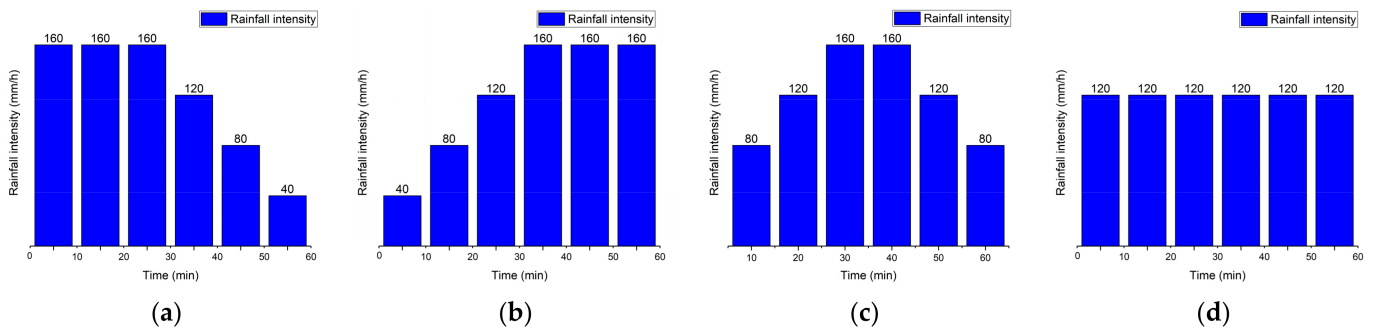
Figure 3. Rainfall patterns: (**a**) Pattern I; (**b**) Pattern II; (**c**) Pattern III; (**d**) Pattern IV.

Table 2. Soil composition.

Soil Type	Clay (%)	Silt (%)	Sand (%)	Gravel (%)	D_{50} (mm)	Initial Volume Moisture Content (%)	Initial Dry Density (g/cm³)
Silty soil	10.2	68.6	21.2	0	0.021	9.1	1.88
Sandy soil	7.1	18.5	74.4	0	0.71	8.2	1.74
Gravel soil	8.8	16.9	18.6	55.7	2.54	6.5	1.50
Mixed soil	10.2	24.9	36.7	28.2	1.68	7.7	1.61

Figure 4. Grain size distribution curves.

2.3. Test Procedures
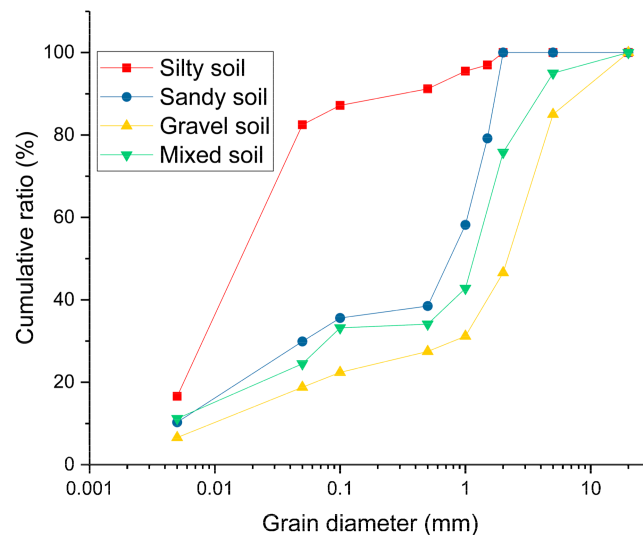
Before the test began, the soil was filled into the flume, with each layer being 10 cm deep. The soil was paved to the same thickness in each layer and then knocked evenly with wood blocks. Measuring instruments were embedded in the positions that are shown in Figure 1. After the preparation was completed, the test started with the commencement of the rainfall. Each rainfall lasted 1 h. At the end of a test, the amount of sediment that was yielded by the landslide was measured.

3. Results

3.1. Slope Instability Processes under Different Rainfall Intensities

When a slope encounters rainfall with different intensities, its water content, matrix suction, pore water pressure, and total stress exhibit different change processes. Water content is a basic parameter that is used to describe soil's properties. The volumetric water content of the tests with higher rainfall intensity were found to rise earlier and the matrix suction declined earlier, too. When the rainfall intensity was 160 mm/h, the volumetric water content reached its maximum at about 40 min. When the rainfall intensity was 120 mm/h, the volumetric water content reached its maximum at about 55 min. The water gradually penetrated downward from the soil's surface, so the volumetric water content deeper down within the soil was found to increase later than that of the position near the surface.

Matrix suction is an important parameter of the mechanical properties of unsaturated soils. The pores of unsaturated soil are filled with water and air. The water–air interface has surface tension. In unsaturated soil, through capillary action, the pore water pressure under the bent liquid surface is less than the pore air pressure. The shrinkage membrane is subjected to air pressure greater than the water pressure, and this pressure difference is called matrix suction. The processes of matrix suction that were observed at the different depths under the different rainfall intensities are shown in Figure 5b. It can be seen from the figure that the change curve of matrix suction was divided into three stages, namely the initial stage, steep fall stage, and stable stage. Taking, as an example, the matrix suction change process that was observed at position I when the rainfall intensity is 160 mm/h, it was noted that within 22 min of the beginning of rainfall, the change in the soil matrix suction was not obvious. At 22–42 min, the matrix suction of the slope soil decreased abruptly. As the infiltration of the rainfall continued to increase, the soil matrix suction decreased to the minimum and became stable.

Pore water pressure is the pressure of the groundwater that is present in soil or rock, which acts between particles or pores and is an important indicator of stress changes in the soil. The variation of pore water pressure that was observed at the different slope locations under the different rainfall intensities is shown in Figure 5c. The pore water pressure variation curves during the test were observed in three stages: the initial stage, surging stage, and slowly increasing stage. It was specifically noted that a greater intensity of rainfall led to a shorter duration of the initial stage. For example, the initial stage of pore water pressure at position I lasted about 8 min when the rainfall intensity was 160 mm/h, and about 24 min when the rainfall intensity was 40 mm/h.

The total stress is the total force per unit area that is acting within a mass of soil. It increases with the greater depth of the measurement point. Different rainfall intensities lead to different variation processes of total stress. When the rainfall intensity was small, the total stress started to increase a short time after the rainfall began and the increase process was relatively smooth. When the rainfall intensity was higher, the total stress started to increase at the beginning of the rainfall.

The intensity of the rainfall is closely related to the occurrence of a landslide. When the intensity of rainfall was 40 mm/h and 80 mm/h, no landslide occurred. For the case of a rainfall intensity of 120 mm/h, the time of the initial landslide occurrence was about 47 min. For the case of a rainfall intensity of 160 mm/h, the time of the initial landslide occurrence was about 40 min.
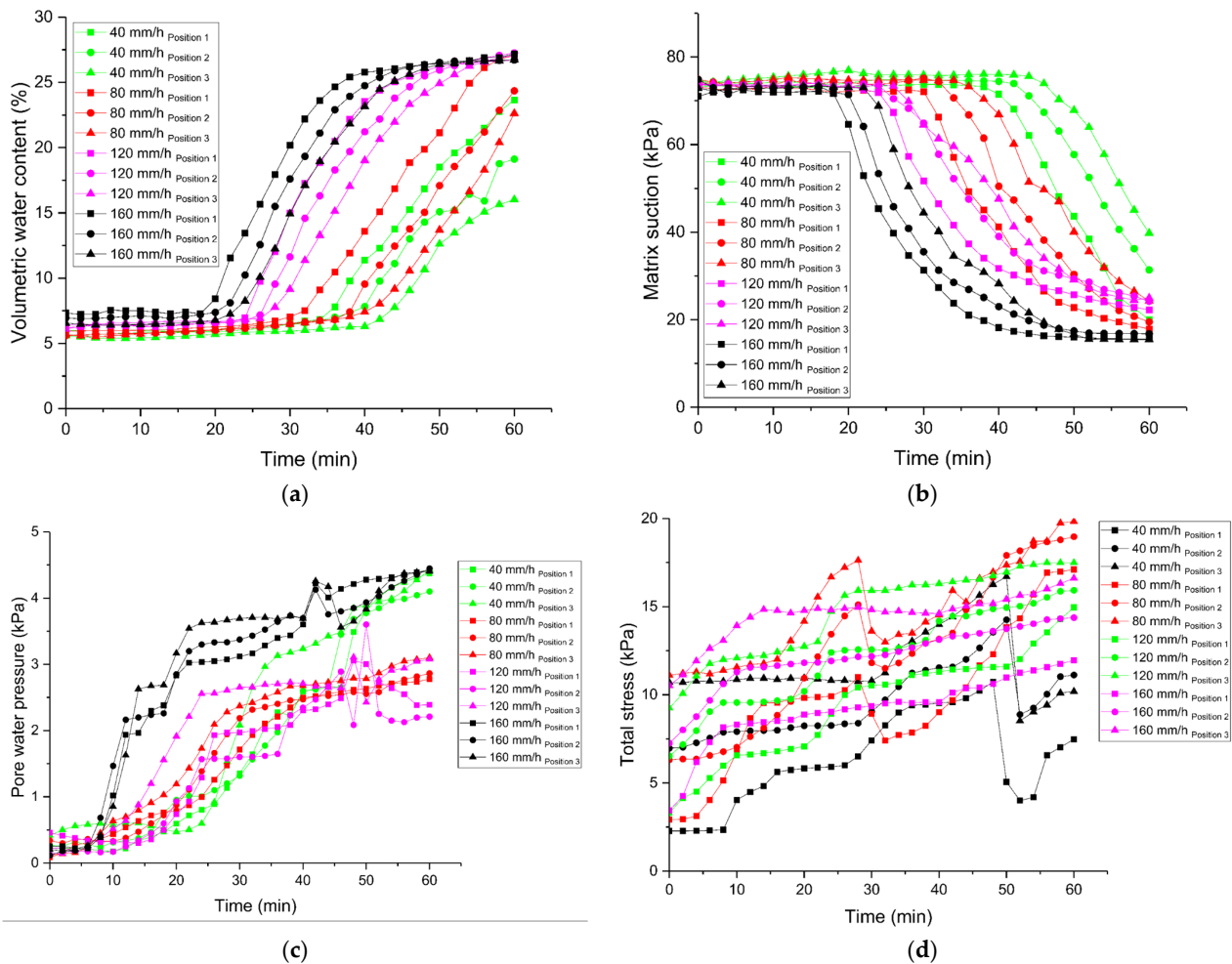
Figure 5. Variation in measured data when rainfall intensity is different: (**a**) water content; (**b**) matrix suction; (**c**) pore water pressure; (**d**) total stress.

3.2. Slope Instability Processes under Different Rainfall Patterns

The changes in the water content, matrix suction, pore water pressure, and total stress that were observed under the different rainfall patterns are shown in Figure 6. The volumetric water content that was measured at the measurement points did not change for a period of time after the onset of rainfall. The volumetric water content of rainfall pattern I started to increase at the earliest time point. Later, the volumetric water content of rainfall patterns IV and III started to increase. The volumetric water content of rainfall pattern II started to increase last. The rate of the increase in the volumetric water content in the rainfall pattern I test decreased gradually. The rate of increase in the rainfall pattern IV test remained constant. The rate of increase in rainfall pattern II and rainfall pattern III gradually increased.

The matrix suction of the tests with rainfall pattern I and rainfall pattern IV began to diminish earlier than the matrix suction of pattern II and pattern III. The matrix suction curve of the tests with rainfall pattern I and rainfall pattern IV began to enter the attenuation stage at about 20 min, while those of pattern II and pattern III began to enter the attenuation stage at about 35 min. The rainfall of patterns I and IV was relatively large in the initial stage. The attenuation processes of these tests were similar. In the stable stage, the matrix suction of the test with patterns I and IV was the smallest, and those of patterns II and III were relatively large.

In the changing process of pore water pressure, the slow-changing stages of the rainfall pattern I and IV tests lasted the shortest time. The rate of the curve was very large at the beginning. After the surge stage, it tended to be smooth. The slow change phase of rainfall

patterns II and III lasted longer and the pore water pressure increased slowly throughout the test process. As the rainfall continued, the rainfall intensity of rainfall patterns II and III gradually increased and the pore water pressure changed into the surge stage. The pore water pressure of rainfall patterns I, III, and IV increased slightly in the stable stage.
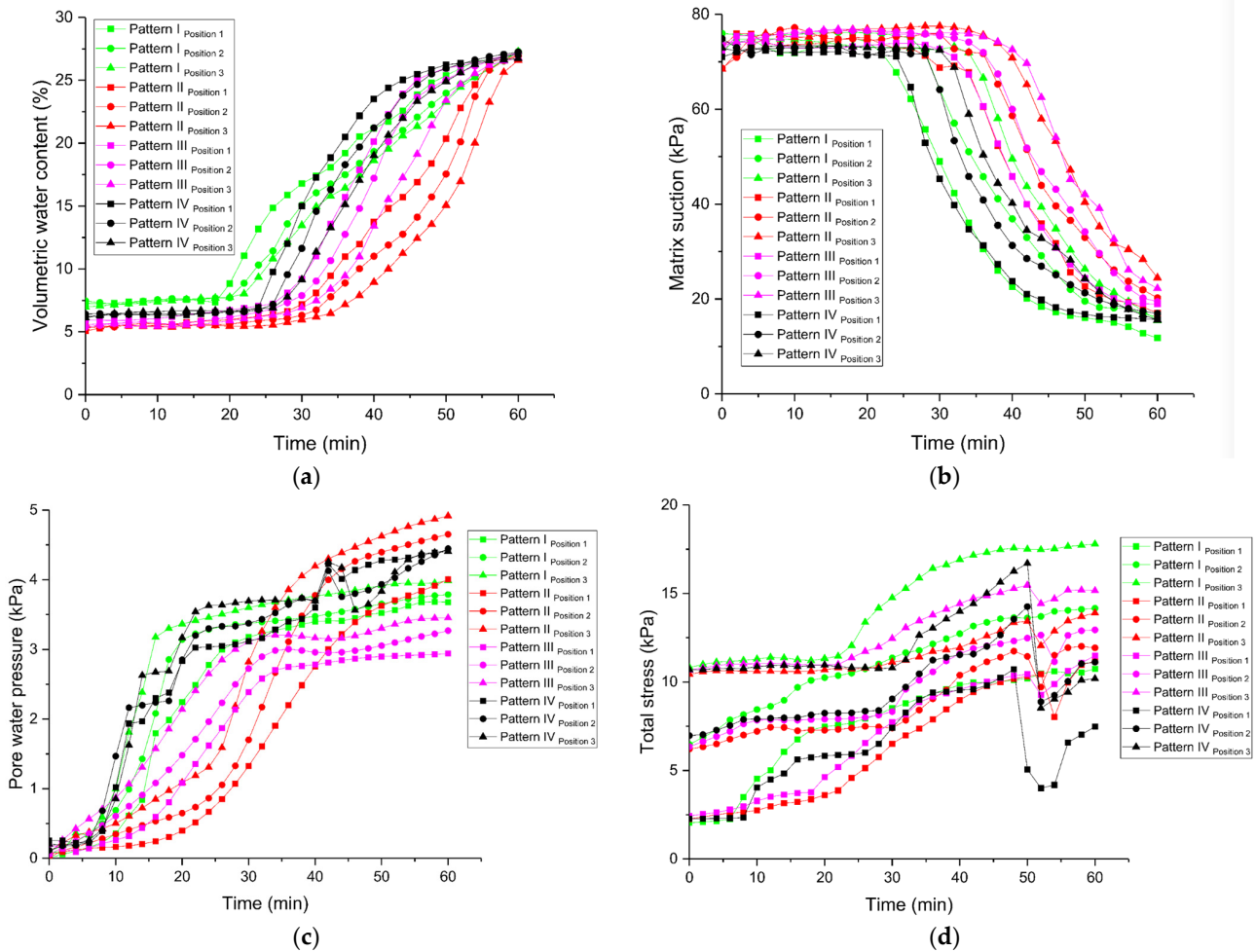

Figure 6. Variation in measured data when rainfall patterns are different: (**a**) water content; (**b**) matrix suction; (**c**) pore water pressure; (**d**) total stress.

Different rainfall patterns cause different response processes of total stress. The soil response under rainfall pattern I was rapid. The total stress began to rise at 5 min. The growth rate slowed down at about 20 min. The total stress of the tests with rainfall pattern II and rainfall pattern III began to increase by close to the 20 min mark. Compared with rainfall pattern I, these patterns displayed lag. The total stress of the tests with rainfall patterns II and IV suddenly decreased in the later rainfall stage, due to the landslide.

The occurrence of landslides varied under the different rainfall patterns: no landslides occurred in rainfall pattern I, while landslides did occur in rainfall patterns II, III, and IV. The first landslide of the test with rainfall pattern II occurred at about 42 min. The first landslide of the test with rainfall pattern III occurred at about 45 min. The first landslide of the test with rainfall pattern IV occurred at about 47 min.

3.3. Slope Instability Processes with Different Soil Types

Figure 7 shows the variation of water content, matrix suction, pore water pressure, and total stress of the slopes with different soil compositions. For the same rainfall intensity, there was no significant difference in the time at which the volumetric water content started to rise for the different soils. The volumetric water content for all of them started to increase

at about 25 min. However, there were large differences in the final volumetric water content of the different soil types. The upper limit of the volumetric water content was the highest for the silty soil, at about 36%. The upper limit of the volumetric water content for the mixed soil was about 30%. The sandy soil had an upper volumetric water content of about 27%. The gravel soil had the lowest upper limit of volumetric water content, which was about 18%. The volumetric water content of the silty and mixed soils rose very quickly and reached their maximum water content at about 35 min. The volumetric water content of the sandy soil rose over a longer period of time and the rate gradually decreased. The volumetric water content of the gravel soil plateaued after a small increase.
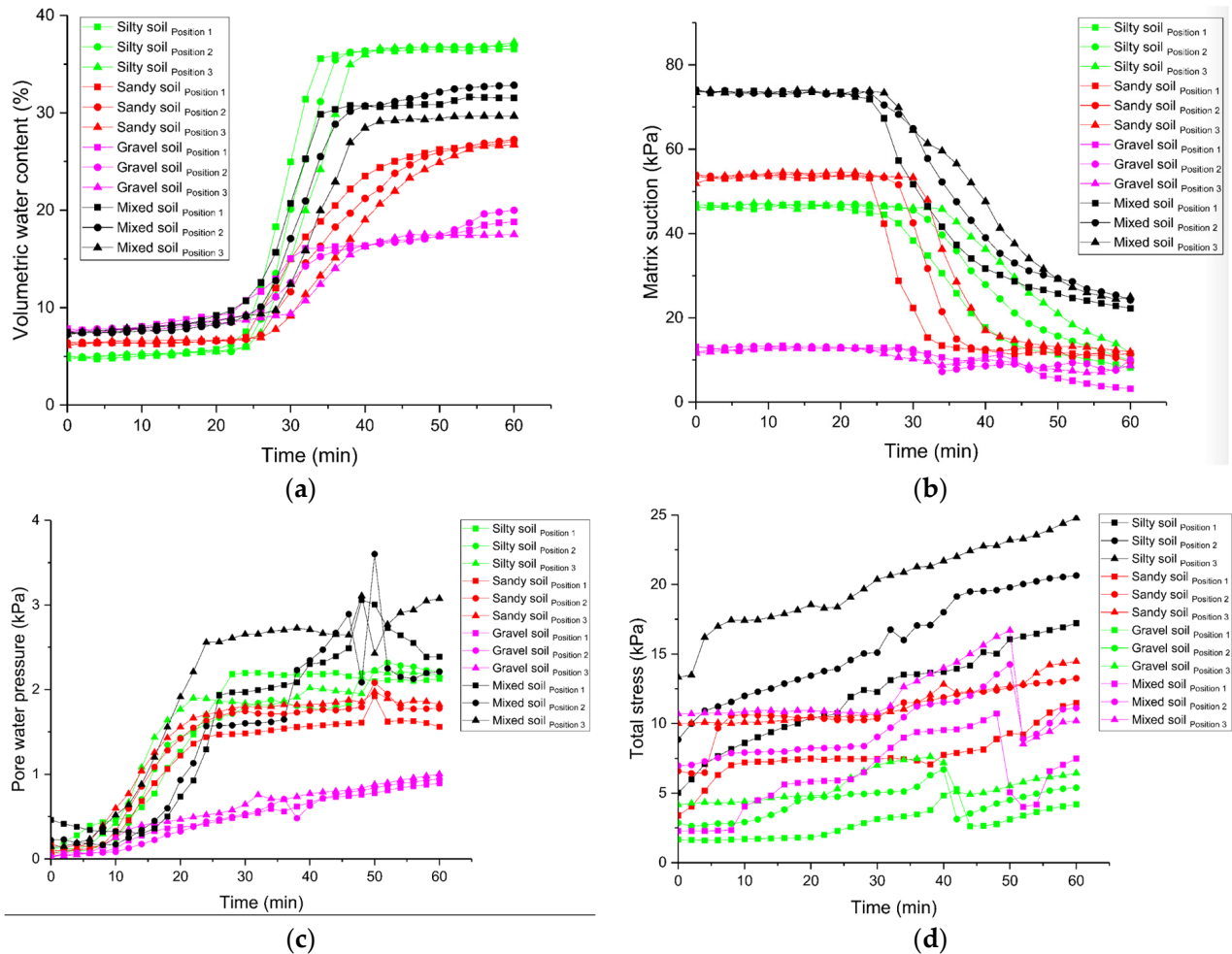

Figure 7. Variation in measured data when soil types are different: (**a**) water content; (**b**) matrix suction; (**c**) pore water pressure; (**d**) total stress.

The initial matrix suction of the different soils showed great differences. The initial matrix suction of the fine-grained soils was higher than that of the coarse-grained soils. The initial matrix suction of the silty soil was about 78 kPa, that of the sandy soil was about 52 kPa, that of the gravel soil was only about 14 kPa, and that of the mixed soil was about 48 kPa. The changing processes of matrix suction were also different. The matrix suction of the silty soil at location I entered the diminished stage at about 28 min, decreased sharply in the time period of 30 ~ 40 min, and finally stabilized at about 20 kPa. The matrix suction of the sandy soil and mixed soil decreased at about 25 min and the matrix suction of the sandy soil reached the stable stage at 35 min with a value of 18 kPa. The matrix suction of the mixed soil continued to decline and finally decreased to about 8 kPa. The matrix suction of the gravel soil was very small and did not change significantly in the first 30 min of rainfall. It entered the fluctuating stage at 30 min.

The soil type had a strong influence on the changing process of pore water pressure. The increasing process of pore water pressure was longer for the mixed soil. The peak occurred between 30 and 40 min and it reached about 4 kPa. The pore water pressure changes that were observed in the silty, sandy, and gravel soils can be divided into two stages: a rapid-increase stage and a stable stage. The increasing stage was seen in approximately the first 20 min of the test. When the increasing stage was over, the pore water pressure of the silty soil was greater than that of the sandy soil, and that of the sandy soil was greater than that of the gravel soil.

The different soil types had different total stress values. At position I, the total stress was highest in the silty soil. It increased slowly during the time period from 10 to 40 min and remained constant at about 10 kPa during the time period from 40 to 60 min. The total stress of the sandy soil varied little in the first 20 min, increased and fluctuated in the time period from 20–50 min, and decreased abruptly at about 50 min due to the landslide. The total stress of the gravel soil was the smallest and it increased only slightly during the rainfall and then stabilized around 4 kPa. The total stress variation pattern of the mixed soil was similar to that of the sandy soil.

Soil type is a key factor for determining the stability of slopes. Under the fixed rainfall process and slope conditions that were set in these tests, no landslide occurred when the soil type was silty or sandy. Landslides were generated when the soil type was gravelly or mixed. The initial landslide occurrence time was about 39 min for the gravel soil and about 47 min for the mixed soil.

3.4. Slope Instability Processes on Differently Angled Slopes

Figure 8 shows the variation process of matrix suction when the slope gradients were different. The different slope gradients had little influence on the variation of the volume water content, the variation of each test was generally similar. The rise speed rate of the 30° slope was less than that of the 5° slope and 15° slope.

The changing process of the matrix suction of the different gradient slopes was generally similar. For example, in a test with a 30° slope at position I it was observed that, in the first 25 min of rainfall, the change in the matrix suction was not obvious. At 26–46 min, the matrix suction at this location decreased abruptly. As the infiltration of the rainfall continued to increase, the soil matrix suction dropped to the minimum level and then stabilized. Since the precipitation on the steep slope was largely converted into surface runoff during the rainfall-infiltration process, the infiltration volume was smaller than that of the gentle slope at the same time. The matrix suction started to decrease earlier for the tests on the gentle slope than those on the steep slope.

The increasing and stable stages of pore water pressure on the slopes with different gradients had large differences. Taking location I as an example, when the slope was gentle (5°), the rising curve of the pore water pressure resembled a convex function. That is, the function slope was larger at the beginning and the period from 5–12 min accommodated the concentrated rising section of the pore water pressure process. When the slope was 15°, the growth of the pore water pressure was approximately linear. When the slope was 30°, the curve of the pore water pressure increase was similar to the concave function, which decreased slightly in the time period from 0–15 min and increased rapidly in the time period from 20–25 min. In the stable stage, the pore water pressure on the 15° slope was the largest, around 3.2 kPa. The pore water pressure on the 30° slope was about 2.5 kPa and the pore water pressure on the 5° slope was stable at about 2.8 kPa.

The slope had a significant effect on the changing process of the total stress. For the case of a 5° slope, the total stress at position I and position II increased linearly throughout the test. For the case of the 15° slope, the total stress at position II changed very little in the first 25 min, increased significantly in the time period from 25 to 45 min, and suddenly decreased at about 47 min due to a landslide. For the case of the 30° slope, the total stress changed little in the first 40 min at position II, increased continuously from 40 min, and decreased suddenly at around 50 min due to the landslide.
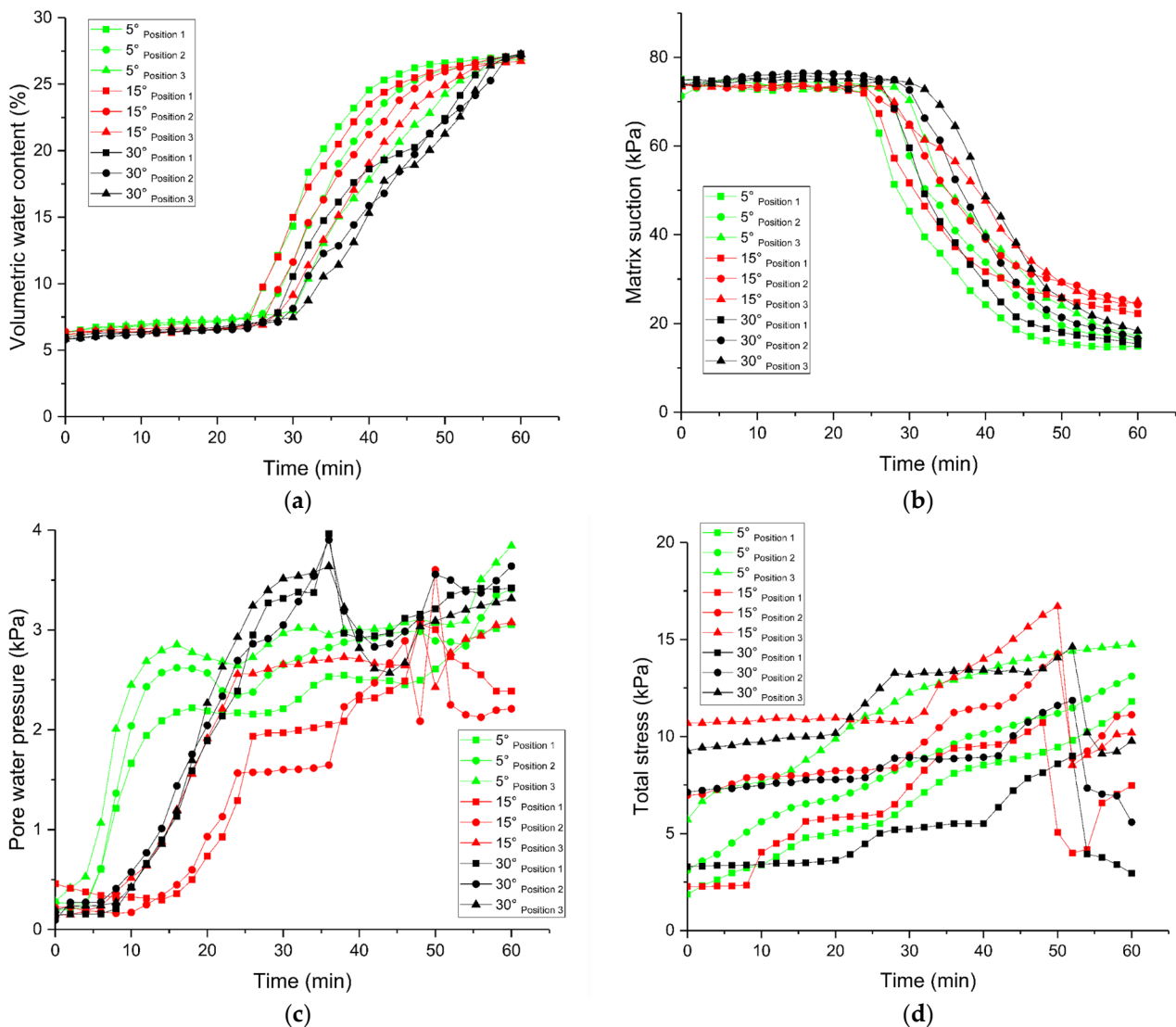
Figure 8. Variation in measured data when slope gradients are different: (**a**) water content; (**b**) matrix suction; (**c**) pore water pressure; (**d**) total stress.

The gradient of the slope was a decisive factor for the occurrence of landslides. No landslide occurred on the 5° slope. Landslides occurred on both the 15° and 30° slopes. The initial landslide occurred at about 47 min on the 15° slope and about 33 min on the 30° slope.

4. Discussion

A series of physical model tests for rainfall-induced shallow slides have been carried out then and reported on in this paper. The soil samples were made according to the natural soil in the Min Jiang River basin in southwestern China. The different soil types have unique characteristics. Silty soils are usually well-aggregated, but the aggregates break down rapidly when wetted, allowing non-aggregated soil particles to be easily transported [42]. For sandy soil, there is a clear linkage between landslides and sediment yield [43]. Seismic activity will generate a large amount of gravel soils and make the region susceptible to geohazards [22]. Therefore, the impact of the typical soil constitution on the landslides and sediment yield is analyzed in this paper. The sediment yield of the landslides that resulted from tests with different rainfall intensities, rainfall patterns, slope gradients, and soil particle compositions is shown in Table 3. All of the soil that slid down came from within 10 cm of the surface layer of the original mass, so the mass of the soil

that slid down by landslide, as a percentage of the total mass of the upper 10 cm layer of the original slope, was used to measure the severity of the landslide.

Table 3. Sediment yield from landslides.

Test No.	Slope (°)	Rainfall Intensity (mm/h)	Rainfall Pattern	Soil Sample	Time of Initial Landslide (min)	Sediment Yield (%)
3	15	120	IV	Mixed soil	47	11.20
4	15	160	IV	Mixed soil	40	18.20
6	15	120	II	Mixed soil	42	14.6
7	15	120	III	Mixed soil	45	12.4
10	15	120	IV	Gravel soil	39	9.80
12	30	120	IV	Mixed soil	33	24.20

Some research on rainfall-induced shallow landslides has been conducted. A comprehensive physics-based Integrated Hydrology Model was set up, which is appliable to different rainfall characteristics [44]. In this paper, more factors are studied in order to investigate the mechanisms of rainfall-induced shallow landslides. The impact of the water content and pore water pressure was analyzed by monitoring a natural slope [45]. However, the variables of that study are not complete because matrix suction and total stress are lacking. A distributed one-dimensional modeling approach for predicting shallow-rainfall-induced landslides was established [46], but the actual landslides are complex. In this paper, more factors have been considered. The influence of soil depth on the occurrence of shallow landslides has been previously investigated [43], but evidence of how the rainfall and soil condition affect a landslide's occurrence is lacking.

The occurrence of landslides and their sediment yield is related to many factors. To investigate the effect of one factor and the following comparisons, the other factors were kept the same. Under a rainfall intensity of 120 mm/h (Test 3), the first landslide occurred at 39 min. Under a rainfall intensity of 160 mm/h (Test 4), the first landslide occurred at 47 min. This suggests that the higher the intensity of rainfall, the earlier the initial landslide occurs. The sediment yield of Test 4 was also larger than that of Test 3. When the rainfall intensity was 80 mm/h, there was no landslide. This indicates that the occurrence of landslides under the test conditions requires the rainfall intensity to exceed 80 mm/h. The rainfall pattern also affected the occurrence of landslides and the first landslide's time of occurrence. In the tests with rainfall patterns II, III, and IV (Test 6, 7, and 3), the first landslides were at 42 min, 45 min, and 47 min, respectively. In the test with rainfall pattern I, no landslide occurred. For the different soil types, the initial landslide occurrence times of the gravel soil and the mixed soil were 39 min and 47 min, and the sediment yields were 9.8% and 11.2%, respectively. No landslide occurred in the silty soil or the sandy soil. Soils composed of coarse grains were shown to be prone to landslides. The landslide on the 30° slope (Test 12) occurred earlier, at 33 min, than those which occurred during all of the tests on the 15° slope. The sediment yield was 24.2%, which was also higher than those on the 15° slope.

5. Conclusions

Landslides are a gravity-driven mass movement and induce an increase in sediment yield in the watershed. In this paper, a series of artificial rainfall tests were conducted in order to investigate rainfall-induced shallow landslides. Four impact factors, including rainfall intensity, rainfall pattern, soil type, and slope gradient, were set to be studied. The changing processes of volumetric water content, matrix suction, pore water pressure, and total stress during rainfall were analyzed. The conclusions were as follows.

The occurrence of rainfall-induced shallow landslides was related to the intensity and pattern of the rainfall, slope gradient, and soil composition. Landslides were triggered by rainfall of a certain intensity and, according to the results obtained from the present tests, the rainfall intensity must exceed 40 mm/h in order to trigger a landslide. The higher

the rainfall intensity, the earlier the landslide occurs. The rainfall pattern also influenced landslide generation.

The variables had unique processes of change during the rainfall that occurred under the different combinations of impact factors. The process of matrix suction consisted of an initial stage, steep decline stage, and stable stage. With greater intensity of rainfall, the matrix suction diminished earlier. The pore water pressure continued to rise through the rainfall and it started to rise earlier when the rainfall intensity was greater. In the tests with different rainfall patterns, matrix suction began to diminish later when the rainfall intensity peaked in the middle or late stage (patterns II and III). On the steep slope, soil water content rose and matrix suction diminished later than on the gentler slopes.

When rainfall-induced shallow landslides occurred, there was a corresponding significant change in the physical parameters of the slope. The landslides occurred after the matrix suction entered the diminished stage. The different soil compositions had sequential landslide occurrence times, with the silty and sandy types occurring earlier than the gravelly and mixed types. The pore water pressure rose briefly before the landslide occurred and fell back down after the landslide occurred. As the landslides caused rapid local soil movement, total stress produced rapid changes during the landslides and, in most cases, obviously decreased.

The sediment yield from the landslides was influenced by various factors. When the intensity of the rainfall increased, the sediment yield increased. The sediment yield of the landslides with coarser particle composition was greater than that of the finer soils. The sediment yield of the 30° slope was significantly higher than that of the 15° slope.

Author Contributions: Conceptualization, Y.L. and X.W.; methodology, Y.L. and X.W.; software, Y.L. and Z.D.; validation, Z.D.; investigation, Y.L. and Z.D.; data curation, Y.L. and Z.D.; writing—original draft preparation, Y.L.; writing—review and editing, Y.L. and X.W.; funding acquisition, X.W. All authors have read and agreed to the published version of the manuscript.

Institutional Review Board Statement: Not applicable.

Informed Consent Statement: Not applicable.

Data Availability Statement: The data presented in this study are available on request from the corresponding author.

Conflicts of Interest: The authors declare no conflict of interest.

References

1. Glade, T.; Anderson, M.G.; Crozier, M.J. *Landslide Hazard and Risk*; John Wiley & Sons: Hoboken, NJ, USA, 2006.
2. Ray, A.; Bharati, A.K.; Rai, R.; Singh, T.N. Landslide occurrences in Himalayan residual soil: A review. *Himal. Geol.* **2021**, *42*, 189–204.
3. Clague, J.J.; Stead, D. *Landslides: Types, Mechanisms and Modeling*; Cambridge University Press: New York, NY, USA, 2012.
4. Chen, Y. *Landslide Disaster*; Seismological Press: Beijing, China, 2020.
5. Yi, X.; Feng, W.; Bai, H.; Shen, H.; Li, H. Catastrophic landslide triggered by persistent rainfall in Sichuan, China: August 21, 2020, Zhonghaicun landslide. *Landslides* **2021**, *18*, 2907–2921. [CrossRef]
6. Wu, Y.; Zhang, M.; Yang, L.; Liu, T.; Zhang, T.; Sun, Q.; Wang, B.; Xie, X. Failure mechanisms and dynamics of the Shanzao rockslide in Yongjia County, China on 10 August 2019. *Landslides* **2021**, *18*, 2565–2574. [CrossRef]
7. Xia, M.; Ren, G.M.; Yang, X.L. Mechanism of a catastrophic landslide occurred on May 12, 2019, Qinghai Province, China. *Landslides* **2021**, *18*, 707–720. [CrossRef]
8. Dikshit, A.; Sarkar, R.; Pradhan, B.; Segoni, S.; Alamri, A.M. Rainfall Induced Landslide Studies in Indian Himalayan Region: A Critical Review. *Appl. Sci.* **2020**, *10*, 2466. [CrossRef]
9. Wang, K.; Zhang, S. Rainfall-induced landslides assessment in the Fengjie County, Three-Gorge reservoir area, China. *Nat. Hazards* **2021**, *108*, 451–478. [CrossRef]
10. Huang, G.; Zheng, M.; Peng, J. Effect of Vegetation Roots on the Threshold of Slope Instability Induced by Rainfall and Runoff. *Geofluids* **2021**, *2021*, 6682113. [CrossRef]

11. Garg, A.; Huang, H.; Kushvaha, V.; Madhushri, P.; Kamchoom, V.; Wani, I.; Koshy, N.; Zhu, H.-H. Mechanism of biochar soil pore–gas–water interaction: Gas properties of biochar-amended sandy soil at different degrees of compaction using KNN modeling. *Acta Geophys.* **2019**, *68*, 207–217. [CrossRef]

12. Chang, J.-M.; Chen, H.; Jou, B.J.-D.; Tsou, N.-C.; Lin, G.-W. Characteristics of rainfall intensity, duration, and kinetic energy for landslide triggering in Taiwan. *Eng. Geol.* **2017**, *231*, 81–87. [CrossRef]

13. Marin, R.J. Physically based and distributed rainfall intensity and duration thresholds for shallow landslides. *Landslides* **2020**, *17*, 2907–2917. [CrossRef]

14. Li, Q.; Huang, D.; Pei, S.; Qiao, J.; Wang, M. Using Physical Model Experiments for Hazards Assessment of Rainfall-Induced Debris Landslides. *J. Earth Sci.* **2021**, *32*, 1113–1128. [CrossRef]

15. Wu, L.Z.; Xu, Q.; Zhu, J.D. Incorporating hydro-mechanical coupling in an analysis of the effects of rainfall patterns on unsaturated soil slope stability. *Arab. J. Geosci.* **2017**, *10*, 386. [CrossRef]

16. Sagitaningrum, F.H.; Bahsan, E. Parametric study on the effect of rainfall pattern to slope stability. *MATEC Web Conf.* **2017**, *101*, 5005. [CrossRef]

17. Buscarnera, G.; Di Prisco, C.P. Soil stability and flow slides in unsaturated shallow slopes: Can saturation events trigger liquefaction processes? *Géotechnique* **2013**, *63*, 801–817. [CrossRef]

18. Li, W.C.; Dai, F.C.; Wei, Y.Q.; Wang, M.L.; Min, H.; Lee, M.L. Implication of subsurface flow on rainfall-induced landslide: A case study. *Landslides* **2015**, *13*, 1109–1123. [CrossRef]

19. Feng, C.; Tian, B.; Lu, X.; Beer, M.; Broggi, M.; Bi, S.; Xiong, B.; He, T. Bayesian Updating of Soil–Water Character Curve Parameters Based on the Monitor Data of a Large-Scale Landslide Model Experiment. *Appl. Sci.* **2020**, *10*, 5526. [CrossRef]

20. Cui, Y.-F.; Zhou, X.-J.; Guo, C.-X. Experimental study on the moving characteristics of fine grains in wide grading unconsolidated soil under heavy rainfall. *J. Mt. Sci.* **2017**, *14*, 417–431. [CrossRef]

21. Chen, N.; Zhou, W.; Yang, C.; Hu, G.; Gao, Y.; Han, D. The processes and mechanism of failure and debris flow initiation for gravel soil with different clay content. *Geomorphology* **2010**, *121*, 222–230. [CrossRef]

22. Liao, L.; Yang, Y.; Yang, Z.; Zhu, Y.; Hu, J.; Zou, D.H.S. Mechanical state of gravel soil in mobilization of rainfall-induced landslides in the Wenchuan seismic area, Sichuan province, China. *Earth Surf. Dyn.* **2018**, *6*, 637–649. [CrossRef]

23. Wang, G.; Sassa, K. Pore-pressure generation and movement of rainfall-induced landslides: Effects of grain size and fine-particle content. *Eng. Geol.* **2003**, *69*, 109–125. [CrossRef]

24. Huang, K.; Duan, H.; Yi, Y.; Yu, F.; Chen, S.; Dai, Z. Laboratory Model Tests on Flow Erosion Failure Mechanism of a Slope Consisting of Anqing Group Clay Gravel Layer. *Geofluids* **2021**, *2021*, 5559052. [CrossRef]

25. Pajalić, S.; Peranić, J.; Maksimović, S.; Čeh, N.; Jagodnik, V.; Željko, A. Monitoring and Data Analysis in Small-Scale Landslide Physical Model. *Appl. Sci.* **2021**, *11*, 5040. [CrossRef]

26. Rahardjo, H.; Lee, T.T.; Leong, E.C.; Rezaur, R.B. Response of a residual soil slope to rainfall. *Can. Geotech. J.* **2005**, *42*, 340–351. [CrossRef]

27. Hou, X.; Li, T.; Qi, S.; Guo, S.; Li, P.; Xi, Y.; Xing, X. Investigation of the cumulative influence of infiltration on the slope stability with a thick unsaturated zone. *Bull. Int. Assoc. Eng. Geol.* **2021**, *80*, 5467–5480. [CrossRef]

28. Chen, H.; Lee, C.F.; Law, K.T. Causative Mechanisms of Rainfall-Induced Fill Slope Failures. *J. Geotech. Geoenvironmental Eng.* **2004**, *130*, 593–602. [CrossRef]

29. Mahmood, K.; Kim, J.M.; Ashraf, M.; Ziaurrehman. The effect of soil type on matric suction and stability of unsaturated slope under uniform rainfall. *KSCE J. Civ. Eng.* **2016**, *20*, 1294–1299. [CrossRef]

30. Cui, P.; Guo, C.-X.; Zhou, J.-W.; Hao, M.-H.; Xu, F.-G. The mechanisms behind shallow failures in slopes comprised of landslide deposits. *Eng. Geol.* **2014**, *180*, 34–44. [CrossRef]

31. Zhan, L.-T.; Guo, X.-G.; Sun, Q.-Q.; Chen, Y.-M.; Chen, Z.-Y. The 2015 Shenzhen catastrophic landslide in a construction waste dump: Analyses of undrained strength and slope stability. *Acta Geotech.* **2021**, *16*, 1247–1263. [CrossRef]

32. Claessens, L.; Knapen, A.; Kitutu, M.; Poesen, J.; Deckers, J. Modelling landslide hazard, soil redistribution and sediment yield of landslides on the Ugandan footslopes of Mount Elgon. *Geomorphology* **2007**, *90*, 23–35. [CrossRef]

33. Al-Sheriadeh, M.S.; Malkawi, A.I.H.; Al-Hamdan, A.; Abderahman, N.S. Evaluating sediment yield at King Talal Reservoir from landslides along Irbid–Amman Highway. *Eng. Geol.* **2000**, *56*, 361–372. [CrossRef]

34. Koi, T.; Hotta, N.; Ishigaki, I.; Matuzaki, N.; Uchiyama, Y.; Suzuki, M. Prolonged impact of earthquake-induced landslides on sediment yield in a mountain watershed: The Tanzawa region, Japan. *Geomorphology* **2008**, *101*, 692–702. [CrossRef]

35. Chuang, S.-C.; Chen, H.; Lin, G.-W.; Lin, C.-W.; Chang, C.-P. Increase in basin sediment yield from landslides in storms following major seismic disturbance. *Eng. Geol.* **2009**, *103*, 59–65. [CrossRef]

36. Bovolo, C.I.; Bathurst, J.C. Modelling catchment-scale shallow landslide occurrence and sediment yield as a function of rainfall return period. *Hydrol. Process.* **2011**, *26*, 579–596. [CrossRef]

37. Bathurst, J.C.; Moretti, G.; El-Hames, A.; Beguería, S.; García-Ruiz, J.M. Modelling the impact of forest loss on shallow landslide sediment yield, Ijuez river catchment, Spanish Pyrenees. *Hydrol. Earth Syst. Sci.* **2007**, *11*, 569–583. [CrossRef]

38. Bathurst, J.C.; Moretti, G.; El-Hames, A.; Moaven-Hashemi, A.; Burton, A. Scenario modelling of basin-scale, shallow landslide sediment yield, Valsassina, Italian Southern Alps. *Nat. Hazards Earth Syst. Sci.* **2005**, *5*, 189–202. [CrossRef]

39. Burton, A.; Bathurst, J.C. Physically based modelling of shallow landslide sediment yield at a catchment scale. *Environ. Earth Sci.* **1998**, *35*, 89–99. [CrossRef]

40. Yang, S.-Y.; Jan, C.-D.; Yen, H.; Wang, J.-S. Characterization of landslide distribution and sediment yield in the TsengWen River Watershed, Taiwan. *Catena* **2019**, *174*, 184–198. [CrossRef]

41. Gan, F.; He, B.; Wang, T. Water and soil loss from landslide deposits as a function of gravel content in the Wenchuan earthquake area, China, revealed by artificial rainfall simulations. *PLoS ONE* **2018**, *13*, e0196657. [CrossRef]

42. Gilley, J.E. Erosion|Water-Induced. In *Encyclopedia of Soils in the Environment*; Hillel, D., Ed.; Elsevier: Oxford, UK, 2005; pp. 463–469.

43. Acharya, G.; Cochrane, T.; Davies, T.; Bowman, E. The influence of shallow landslides on sediment supply: A flume-based investigation using sandy soil. *Eng. Geol.* **2009**, *109*, 161–169. [CrossRef]

44. Ran, Q.; Hong, Y.; Li, W.; Gao, J. A modelling study of rainfall-induced shallow landslide mechanisms under different rainfall characteristics. *J. Hydrol.* **2018**, *563*, 790–801. [CrossRef]

45. Bordoni, M.; Meisina, C.; Valentino, R.; Lu, N.; Bittelli, M.; Chersich, S. Hydrological factors affecting rainfall-induced shallow landslides: From the field monitoring to a simplified slope stability analysis. *Eng. Geol.* **2015**, *193*, 19–37. [CrossRef]

46. Baum, R.L.; Godt, J.W.; Savage, W.Z. Estimating the timing and location of shallow rainfall-induced landslides using a model for transient, unsaturated infiltration. *J. Geophys. Res. Earth Surf.* **2010**, *118*, 1999. [CrossRef]